

The Role of Alkyl Chain Length and Halide Counter Ion in Layered Dion–Jacobson Perovskites with Aromatic Spacers

Algirdas Dučinskas, George C. Fish, Michael A. Hope, Lena Merten, Davide Moia, Alexander Hinderhofer, Loï C. Carbone, Jacques-Edouard Moser, Frank Schreiber, Joachim Maier,* Jovana V. Milić,* and Michael Grätzel*



Cite This: *J. Phys. Chem. Lett.* 2021, 12, 10325–10332



Read Online

ACCESS |



Metrics & More

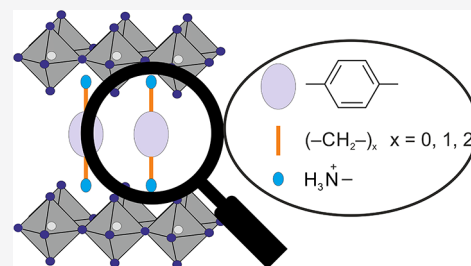


Article Recommendations



Supporting Information

ABSTRACT: Layered hybrid perovskites based on Dion–Jacobson phases are of interest to various optoelectronic applications. However, the understanding of their structure–property relationships remains limited. Here, we present a systematic study of Dion–Jacobson perovskites based on (S)PbX₄ (*n* = 1) compositions incorporating phenylene-derived aromatic spacers (S) with different anchoring ammonium groups and halides (X = I, Br). We focus our study on 1,4-phenylenediammonium (PDA), 1,4-phenylenedimethylammonium (PDMA), and 1,4-phenylenediethylammonium (PDEA) spacers. Systems based on PDA did not form a well-defined layered structure, showing the formation of a 1D structure instead, whereas the extension of the alkyl chains to PDMA and PDEA rendered them compatible with the formation of a layered structure, as shown by X-ray diffraction and solid-state NMR spectroscopy. In addition, the control of the spacer length affects optical properties and environmental stability, which is enhanced for longer alkyl chains and bromide compositions. This provides insights into their design for optoelectronic applications.



Research activity in the field of hybrid halide perovskites has surged over the past decade.^{1,2} These materials are semiconductors with the general formula ABX₃,³ where A is a central cation, which can be methylammonium (MA⁺), formamidinium (FA⁺), Cs⁺, or others; B is a divalent metal ion, such as Pb²⁺, and X is a halide anion (Cl⁻, Br⁻, or I⁻). The optoelectronic properties of hybrid halide perovskites can be controlled by changing the chemical composition or dimensionality.^{4–6} For instance, layered hybrid two-dimensional (2D) perovskites are derived from the conventional three-dimensional (3D) hybrid perovskites by connecting ABX₃ perovskite layers with organic spacer cations.^{7–9} Depending on the valency of the spacer (S) cation and on the packing orientation, layered perovskites are commonly classified into Ruddlesden–Popper (RP) and Dion–Jacobson (DJ) phases. The former is defined by staggered perovskite layers and mostly the (S')₂A_{*n*-1}B_{*n*}X_{3*n*+1} formula, where *n* is the number of perovskite layers separated by the organic spacers and S' is a monovalent spacer cation.¹⁰ On the other hand, the DJ perovskites are often based on the (S)A_{*n*-1}B_{*n*}X_{3*n*+1} formula, where S is a divalent spacer cation, and the layers are stacked without relative displacement.¹¹ While the use of layered perovskites significantly widens the compositional space available for optoelectronic devices, there are several intrinsic problems. The identification of compounds that can be processed into phase-pure 2D perovskite films with suitable structural and optical properties is a key challenge.^{12–14} Depending on the application, environmental stability can also

be an important constraint.¹⁵ Furthermore, due to insulating spacer molecules, the conductivity of these materials is lower as compared to the 3D hybrid perovskites.¹⁶ This can be to some extent circumvented by changing the number (*n*) of perovskite layers, which defines the quantum well thickness and optoelectronic properties.¹⁷ Nonetheless, as *n* increases the phase purity becomes an issue.^{12–14} Moreover, recent work showed that the issue of photoinduced phase instability also affects mixed halide 2D systems.^{18,19}

To address these and other challenges, significant effort has been spent toward the development and investigation of suitable spacers, including aliphatic,^{20–22} aromatic,^{23,24} heterocyclic,^{25,26} and polycyclic aromatic molecules.²⁷ Because of the plethora of spacers available, a holistic understanding of structure–property relationships in layered perovskites is essential to provide material design rules. Typically, when designing a spacer, one should consider its geometry and functional groups, including the core of the spacer (e.g., aromatic moieties), the length of the anchoring group (e.g., alkylammonium chain), and the counterions (e.g., I⁻, Br⁻). According to the previous reports for RP-type layered

Received: September 6, 2021

Accepted: October 11, 2021

Published: October 18, 2021



perovskites, the penetration depth of the anchoring group into the perovskite layers, which correlates with the length of the alkylammonium chain, has a strong effect on structural and optoelectronic properties.^{24,28} Hitherto, the corresponding effect of the length of the anchoring alkylammonium group on the DJ phases is not well understood, despite the importance of the spacer group on the resulting properties.

In this study, we analyze hybrid halide perovskites based on bifunctional 1,4-phenylene-derived analogues of one of the most studied organic spacers, 2-phenethylammonium (PEA),^{29,30} namely 1,4-phenylenediammonium (PDA), 1,4-phenylenedimethylammonium (PDMA), and 1,4-phenylenediethylammonium (PDEA) (Figure 1a). While I-based systems incorporating PDA or PDMA spacers have been previously reported,^{15,31–33} PDEA remains unexplored. To minimize the level of complexity and issues associated with phase purity we focus on $n = 1$ layered perovskite compositions based on iodide and bromide halides (Figure 1b). We demonstrate that the control of the spacer length affects material dimensionality, optical properties, and environmental stability, which is particularly enhanced for longer alkyl chains and bromide compositions.

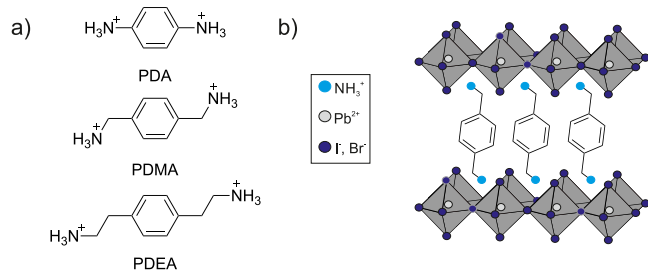


Figure 1. (a) Molecular structures of PDA, PDMA, and PDEA organic spacers. (b) Illustration of layered DJ perovskite structure based on (S)PbX₄ composition.

We studied layered hybrid perovskites based on the (S)PbX₄ ($n = 1$) composition, where S = PDA, PDMA, or PDEA, and X = I or Br. The synthetic procedure is detailed in the [Supporting Information](#) (Section S1). For simplicity, (S)PbX₄ materials based on PDA, PDMA, or PDEA spacers will be denoted as PDA-X, PDMA-X, and PDEA-X, respectively, depending on the halide counterion (X = I, Br). The structure of thin films deposited on glass substrates was investigated by means of X-ray diffraction (XRD). The XRD pattern of PDA-I (Figure 2a, black) corresponds to the (PDA)PbI₄·2H₂O dihydrate (Figure 2a, green), which is a one-dimensional (1D) perovskite, indicating that a layered phase has not formed.³¹ This is likely due to the lack of flexibility of the PDA spacer,³⁴ as well as its lower level of penetration into the neighboring perovskite layers, which prevents the formation of a layered phase.^{21,35} In addition, the PDA-I precursor solution changes its properties over time, which is likely due to the oxidation and subsequent polymerization of (PDA)I₂ (Supporting Information, Section S2, Figures S1 and S2).³⁶ A significant difference in the behavior of the spacer is observed when the alkyl chain length of the spacers is extended by one methylene (–CH₂–) group; the PDMA-I films show typical layered perovskite diffractograms with a sharp diffraction peak at 7.19°, which corresponds to the (001) reflection with a layer spacing of 12.3 Å, along with higher order diffraction peaks of the (00l) Bragg planes family (Figure 2a, red).^{15,32} Further extension of

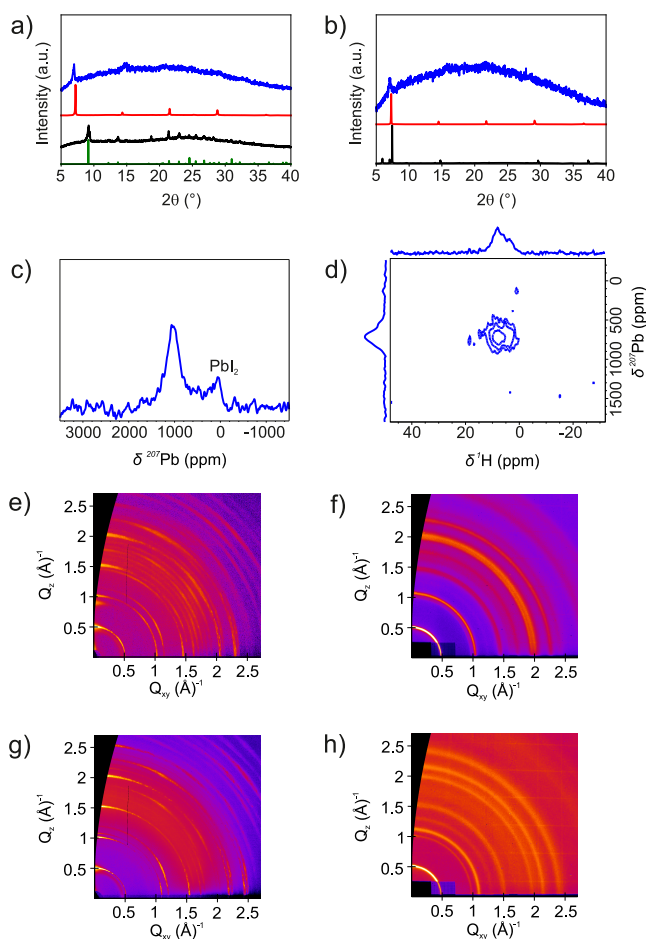


Figure 2. (a,b) X-ray diffraction data of (a) I- and (b) Br-based $n = 1$ layered perovskites: black, PDA; red, PDMA; blue, PDEA. The green line in panel a shows the simulated diffractogram of (PDA)PbI₄·2H₂O (CCDC no. 632922 based on ref 31). (c,d) Solid-state MAS NMR spectra of mechanochemically prepared PDEA-I powder. (c) Room temperature ²⁰⁷Pb spectrum and (d) ²⁰⁷Pb → ¹H HETCOR spectrum at 100 K. Further experimental details are provided in [Section S1](#), [SI](#). (e–h) GIWAXS reciprocal space maps of (e) PDMA-I, (f) PDEA-I, (g) PDMA-Br, and (h) PDEA-Br.

the spacer to PDEA led to a larger lattice parameter, evidenced by the diffraction peak located at 6.98° (Figure 2a, blue), corresponding to a layer spacing of 12.7 Å. However, the crystallinity of the PDEA-I system appears to be lower as compared to PDMA-I, resulting in broader diffraction peaks and the higher order reflections are hardly resolved.³⁷

The XRD patterns of Br-based films (Figure 2b) show the effect of the halide on structural properties. In contrast to PDA-I, the Br-based analogue forms films with the most intense peak at 7.42°, corresponding to d -spacing of 11.9 Å, accompanied by higher order reflections (Figure 2b, black). However, there are two additional peaks below 10° located at 5.90° and 7.0°, which are not attributable to a layered structure. This might be related to the unstable PDA-Br solution (Section S2, Figures S1, S2). In addition, considering previous reports on the corrugated structure of perovskites based on a monofunctional (4-bromophenyl)ammonium spacer,³⁸ which is comparable to PDA, we suspect that the PDA-Br system might form a corrugated structure. As in the I-based systems, extension of the alkyl chain by one methylene resulted in a well-defined layered PDMA-Br material with the

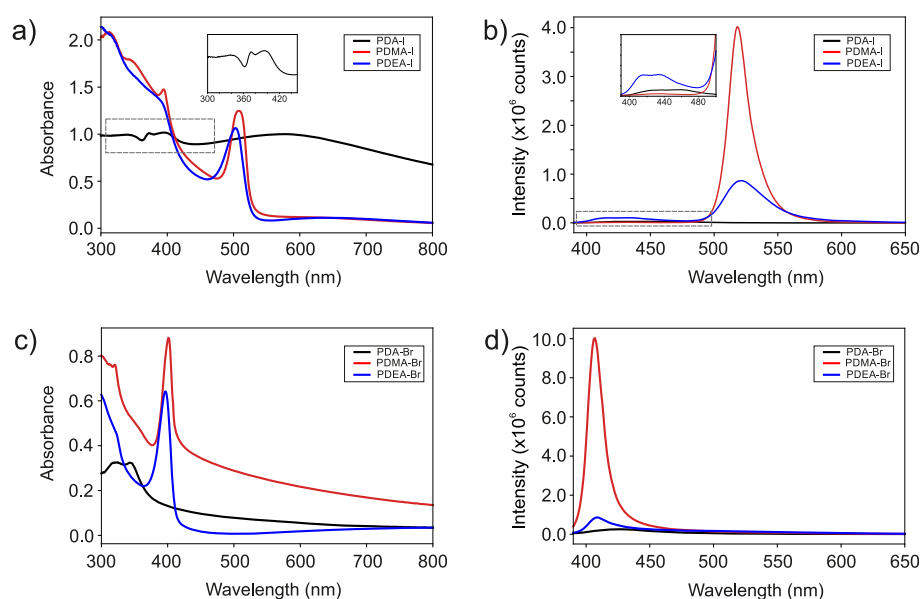


Figure 3. (a,b) UV-vis and steady state PL emission spectra of PDA-I (black), PDMA-I (red), and PDEA-I (blue). The inset in panel a shows zoomed-in absorption in the 300–440 nm range, whereas the inset in panel b represents the zoomed-in emission in the 380–500 nm interval. (c,d) UV-vis and steady-state PL emission spectra of PDA-Br (black), PDMA-Br (red), and PDEA-Br (blue).

basal peak centered at 7.26° (Figure 2b, red), corresponding to *d*-spacing of 12.2 Å. The XRD of PDEA-Br showed only a single broad peak located at 7.01° with a layer spacing of 12.6 Å (Figure 2b, blue), hinting at a lower crystallinity and an increased lattice parameter as compared to PDMA-Br.

Due to the weak diffraction of PDEA-based perovskites, to confirm the formation of a layered structure, mechano-synthesized powders of PDEA-I were studied by solid-state NMR spectroscopy, which is highly sensitive to the local structure and dimensionality of hybrid perovskite systems despite possible differences in morphology compared to thin films (Figure 2c,d and Figures S4–S6).^{39,40} The room temperature ²⁰⁷Pb NMR spectrum (Figure 2c) exhibits a major signal at ~ 1030 ppm, which is characteristic of a 2D $n = 1$ structure,⁴¹ as well as a minor signal at ~ 50 ppm due to unreacted PbI₂. Furthermore, the ²⁰⁷Pb → ¹H HETCOR spectrum recorded at 100 K (Figure 2d) shows a clear correlation between the ²⁰⁷Pb environment in the perovskite layers and the ¹H signals of the PDEA spacer (both the $-\text{NH}_3^+$ signal at ~ 8 ppm and the alkyl signals at ~ 4.5 ppm), proving atomic-scale contact between the two; notably the PbI₂ signal is absent due to the lack of ¹H in this phase. The spectrum was recorded at 100 K to avoid dynamics of the spacer which reduce the efficiency of cross-polarization;⁴² consequently the temperature-dependent ²⁰⁷Pb signal is observed at a lower shift of 720 ppm.^{42,43} The modification of the PDEA cation environment in formation of the layered perovskite can also be seen by the change in the ¹³C NMR signals, particularly those of the alkyl carbons which are closer to the perovskite layers (Figure S4). Taken together, these observations provide strong evidence for the formation of a layered PDEA-I perovskite structure.

To acquire more information about the structure and crystallite orientation, we used synchrotron radiation to perform grazing incidence wide-angle X-ray scattering (GIWAXS) measurements (Figure 2e–h).⁴⁴ While in the samples of PDMA-based perovskites (Figure 2e,g) a well-ordered out-of-plane stacking was indicated by pronounced intensity maxima of the scattering signal in the vertical

direction, ring-like signals were observed for the PDEA systems (Figure 2f,h). These reveal a random orientation of crystallites with no preferred stacking orientation, which is in accordance with the XRD data that probe the vertical direction and, therefore, yield a much larger signal for the well-ordered layered structure as opposed to the randomly oriented crystallites. I- and Br-systems showed the same orientation of crystallites, and the layer spacings obtained from GIWAXS are consistent with those from XRD (Table S1). Both methods show a trend of increasing layer spacing with longer spacer molecules, in accordance with the expectations. Moreover, I-systems had a slightly larger unit cell than Br-systems due to the larger ionic radius. For the PDA-based films, the difficulties to form a layered phase are further apparent (Figure S3). In summary, PDMA and PDEA spacers form thin films with 2D structures, while increasing the spacer length from PDMA to PDEA results in a more isotropic distribution in crystallite orientation for both I- and the Br-based materials.

We thereafter investigated the role of alkyl chain length in the optical properties by UV-vis absorption and of steady state photoluminescence (PL) spectroscopy. The absorption of RP-type $n = 1$ perovskites can be modulated by controlling the length of the organic spacer; shorter spacers reduce the exciton absorption energy.^{24,45,46} The variations in the alkyl chain length change the potential barrier width between lead halide layers⁴⁷ and further affect the perovskite structure by inducing octahedral tilting.²⁴ This is particularly important as the optical properties of layered perovskites are influenced by the Pb–X distances, Pb–X–Pb angles,⁴⁸ and quantum and dielectric confinement.⁴⁹ Typically, $n = 1$ layered perovskites based on Pb and I feature exciton peaks at around 500 nm (~ 2.5 eV), which can be detected at room temperature due to the strong exciton binding energy ($E_b \gg kT$).⁵⁰ This is clearly demonstrated in the optical absorption spectra of the films (Figure 3a), which show pronounced peaks for both PDEA-I and PDMA-I samples at 503 and 508 nm, respectively, in accordance with the reduced alkyl chain length. One would expect an even further exciton absorption energy reduction in

the PDA-based perovskites if they formed well-defined layered perovskites. Instead, we observe a resonant absorption at 380–400 nm, which is attributed to the 1D iodoplumbates.⁵¹

The emission maxima of the PDMA-I and PDEA-I samples are located at 518 and 522 nm (Figure 3b). The larger Stokes shift in PDEA-I might be associated with energy loss via vibrational relaxation and it could also be influenced by higher structural disorder, consistent with the increase in the PL peak width upon extending the alkyl chain of the spacer (Figure S7).^{38,52} The broad emission detected in PDEA-I in the 400–500 nm range might originate from surface species, such as intermediate 1D iodoplumbate phases,^{15,51} given the similarity to the PDA-I emission (Figure 3b, inset). The substitution of I with Br resulted in wider PDMA-Br, PDEA-Br optical bandgaps with excitonic peaks centered at 401 and 397 nm, respectively (Figure 3c). The long absorption tail in the PDMA-Br sample might be attributed to the high surface roughness. For the PDA-Br, an absorption peak at \sim 350 nm suggests that carriers are not solely confined in 2D structures. The emission properties of Br-based films reveal that the PL peaks of both PDMA-Br and PDEA-Br are centered at 407–408 nm, whereas PDA-Br has a very broad emission in the 400–500 nm region (Figure S7). As in the I-based systems, PDEA-Br thin films exhibit a larger Stokes shift and emission bandwidth as compared to PDMA-Br (Figure S7). While both PDMA- and PDEA-based 2D perovskite films feature pronounced excitonic optical absorption and emission, a sharper emission for the PDMA systems is likely related to a higher structural homogeneity, resulting from the more oriented grain distribution compared to PDEA.

To gain more insights into the role of alkyl chain length with regard to charge carrier dynamics, we performed transient absorption (TA) spectroscopy measurements (Figure 4a,c). We focus our analysis on the I-based samples due to setup limitations in the UV region. The TA spectra of PDMA-I and PDEA-I (Figure 4b,c) display similar features, consisting of a negative photobleaching signal at 500 and 510 nm, respectively, as well as two positive features. The presence of a single photobleaching signal indicates an $n = 1$ phase with no higher order phases being present.¹⁴ On the other hand, the PDA-I TA spectrum shows no appreciable features (Figure 4a), further demonstrating the absence of a layered $n = 1$ structure in this system. The shape of the signal in both the PDMA-I and PDEA-I spectra appears to closely match that of the second derivative of the absorption spectra, shown by the dashed black line, which allows us to conclude that the positive features arise due to a photoinduced Stark effect. Stark effects, first evidenced in hybrid perovskite materials in 2014,⁵³ and subsequently in 2D-perovskites^{54,55} and perovskite nanocrystals,⁵⁶ arise due to a change in the absorption of a material in the presence of an electric field; in the case of the photoinduced Stark effect, the electric field is a photoinduced (local) field. The photoinduced signal, ΔA , has been shown to comprise a linear combination of the first and second derivatives of the absorption spectrum.⁵⁷ Changes in the dipole moment are associated with the second derivative of the absorption spectrum, whereas changes in the polarizability of the sample are associated with the first derivative.⁵⁵ Therefore, in the PDMA-I and PDEA-I samples the photoinduced Stark effect arises due to a change in the dipole moment, caused by the photogeneration of charge transfer (CT) excitons. Kinetic traces of the Stark effect feature reveal that the lifetime of CT excitons is comparable between the samples; this implies that

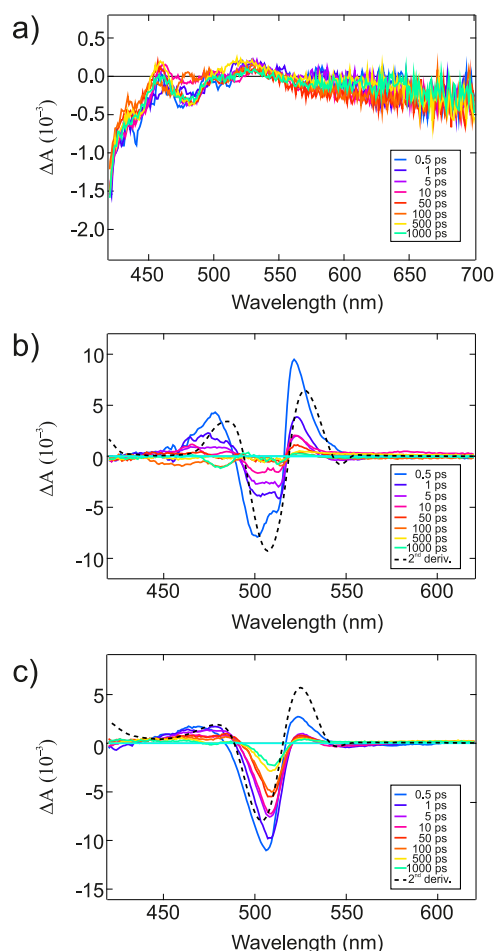


Figure 4. Transient absorption spectra of (a) PDA-I, (b) PDMA-I, and (c) PDEA-I. Samples were excited at 389 nm with a fluence of $23.2 \mu\text{J cm}^{-2}$ (PDA-I) and $3.26 \mu\text{J cm}^{-2}$ (PDMA-I and PDEA-I). The dashed black line corresponds to the second derivative of the absorption spectrum.

the time constant for exciton separation into free charges will be similar between the two samples (Figure S8). The Stark effect feature appears to be larger in the PDMA-I sample, when compared to the PDEA-I, which might be rationalized by the shorter spacer length and smaller layer spacing, resulting in a stronger electric field due to the charge transfer exciton across the layers. Furthermore, layered perovskites have been shown to form multiple quantum well structures,⁵⁸ and tunnelling between these structures can also increase the contribution of the second derivative to the TA signal,⁵⁵ which stimulates a follow-up investigation.

Finally, we investigated the effect of alkyl chain length on the stability of thin films in humid atmosphere. We have previously demonstrated that the PDMA-I system hydrates within minutes when exposed to $\geq 65 \pm 5\%$ relative humidity (RH).¹⁵ We further extended the analysis of the environmental stability to other DJ perovskites by exposing the samples to $70 \pm 5\%$ relative humidity (RH) atmosphere for 20 min at 28 °C. Humidity-treated PDA-I samples did not change the structural (Figure 5a) and optical properties (Figures S9a and S10a), which is expected since the pristine structure is already a dihydrate phase. In contrast, the Br analogue changed its structure (Figure 5d) and new diffraction peaks emerged below 10° , while the optical properties did not change remarkably

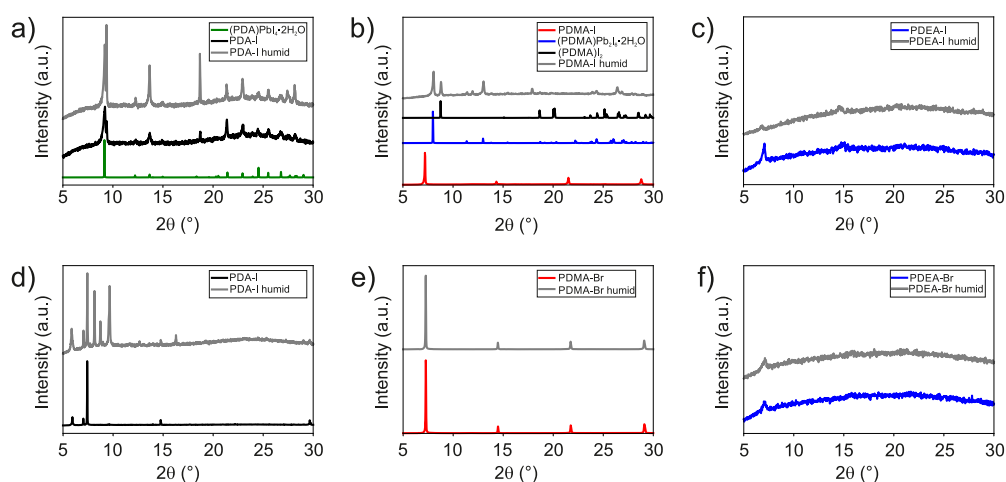
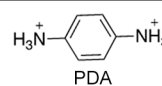
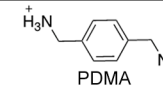
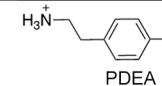


Figure 5. X-ray diffractograms of (a) pristine (black) and hydrated (gray) PDA-I films and the calculated pattern for $(\text{PDA})\text{PbI}_4 \cdot 2\text{H}_2\text{O}$ (green);³ (b) pristine (red) and hydrated (gray) PDMA-I films, and the calculated patterns for $(\text{PDMA})\text{Pb}_2\text{I}_6 \cdot 2\text{H}_2\text{O}$ (blue) and $(\text{PDMA})\text{I}_2$ (black);⁴ (c) pristine (blue) and humidity-treated (gray) PDEA-I films. Diffraction patterns of Br-based samples using PDA, PDMA and PDEA spacers are shown in panels d, e, and f, respectively.

Table 1. The Formation of a Layered Structure, Hydration Stability, and Absorption (A) and Emission (PL) Wavelengths Based on PDA-X, PDMA-X and PDEA-X Systems (X = I, Br)

	 PDA				 PDMA				 PDEA			
Br	2D ^a	Hyd. ^b	A	PL	2D ^a	Hyd. ^b	A	PL	2D ^a	Hyd. ^b	A	PL
			–	–			401 nm	407 nm			397 nm	408 nm
I	2D ^a	Hyd. ^b	A	PL	2D ^a	Hyd. ^b	A	PL	2D ^a	Hyd. ^b	A	PL
			–	–			508 nm	518 nm			503 nm	522 nm

^aThe feasibility to acquire well-defined layered perovskite thin films. Green = formed layered perovskite; gray = possibly formed a layered perovskite but not well-defined; red = did not form layered perovskites. ^bEnvironmental stability with regard to hydration during a 20 min exposure to $70 \pm 5\%$ RH. Green = stable; gray = already hydrated; red = unstable.

(Figures S9b and S10b). In contrast, the optical absorption and emission of PDMA-I, which transforms from a 2D into a 1D structure (Figure 5b),¹⁵ change significantly (Figures S9c and S10c). The replacement of I^- with a Br^- counterion has a significant effect on the propensity of PDMA-based systems to hydrate, as the crystal structure was retained in the PDMA-Br sample upon exposure to humid conditions (Figure 5e). This might be associated with the contracted lattice, which hampers water intercalation into the crystal structure,⁵⁹ or stronger hydrogen bonds between Br and the spacer molecules.^{60–62} Humidity-treated PDEA-I and PDEA-Br revealed no changes in the corresponding diffraction patterns (Figure 5c,f) and the optical properties (Figures S9e–f and S10e–f), confirming that PDEA-I and PDEA-Br maintain a layered structure.^{61,62} Contact angle measurements revealed an improvement in hydrophobicity with increased alkyl chain length of I-based films, whereas Br-based films were not necessarily more hydrophobic (Figure S11), suggesting that other factors might play a role.

All in all, the length of the organic spacer and the counterion affect the stability of DJ perovskites as well as structural and optoelectronic properties (Table 1). While extended spacer systems and Br-based analogues provide enhanced stabilities, they may however affect the resulting charge carrier mobilities

and conductivities of the resulting materials, which remain to be assessed.

In summary, we investigated Dion–Jacobson layered perovskite phases based on phenylene-derived aromatic spacers (S) with different length alkyl chains (i.e., PDA, PDMA, and PDEA) and halide counterions (X = I, Br) of $(\text{S})\text{PbX}_4$ ($n = 1$) composition. The systems based on the PDA spacer did not form a well-defined layered structure. Instead, we demonstrated that PDA-I forms a hydrated 1D structure. The extension of the alkyl chains in the PDMA and PDEA spacers rendered them compatible with the formation of layered perovskite structures, as evidenced by X-ray diffraction and solid-state NMR spectroscopy. Moreover, GIWAXS measurements revealed that in PDMA-based perovskites crystallites are oriented in the out-of-plane directions, whereas there is no preferred stacking orientation in PDEA thin films. Optical bandgap and the emission bandwidth also increase with length of alkyl chain. Moreover, the analysis of charge carrier dynamics by transient absorption spectroscopy revealed in PDMA-I and PDEA-I films a photoinduced Stark effect, which arises due to photogeneration of CT excitons and is related to the length of alkyl chain. Finally, the resilience against moisture increases with the length of the alkyl chain, and the substitution of iodide with bromide also proved to be an effective strategy to enhance stability against humidity.

These results provide critical insights into material design, offering new strategies for tuning the properties of these materials for optoelectronic applications.

■ ASSOCIATED CONTENT

SI Supporting Information

The Supporting Information is available free of charge at <https://pubs.acs.org/doi/10.1021/acs.jpcllett.1c02937>.

Materials and methods, PDA solution instability and its effect on thin-film properties, NMR spectroscopy, PL analysis, transient absorption spectroscopy, supplementary optical data, contact angle measurements (PDF)

■ AUTHOR INFORMATION

Corresponding Authors

Joachim Maier – Max Planck Institute for Solid State Research, Stuttgart 70569, Germany; orcid.org/0000-0003-2274-6068; Email: jmaier@fkf.mpg.de

Jovana V. Milić – Laboratory of Photonics and Interfaces, École Polytechnique Fédérale de Lausanne, Lausanne 1015, Switzerland; Adolphe Merkle Institute, University of Fribourg, Fribourg 1700, Switzerland; orcid.org/0000-0002-9965-3460; Email: jovana.milic@epfl.ch

Michael Grätzel – Laboratory of Photonics and Interfaces, École Polytechnique Fédérale de Lausanne, Lausanne 1015, Switzerland; orcid.org/0000-0002-0068-0195; Email: michael.gratzel@epfl.ch

Authors

Algirdas Dučinskas – Laboratory of Photonics and Interfaces, École Polytechnique Fédérale de Lausanne, Lausanne 1015, Switzerland; Max Planck Institute for Solid State Research, Stuttgart 70569, Germany

George C. Fish – Photochemical Dynamics Group, École Polytechnique Fédérale de Lausanne, Lausanne 1015, Switzerland

Michael A. Hope – Laboratory of Magnetic Resonance, École Polytechnique Fédérale de Lausanne, Lausanne 1015, Switzerland; orcid.org/0000-0002-4742-9336

Lena Merten – Institut für Angewandte Physik, Universität Tübingen, Tübingen 72076, Germany

Davide Moia – Max Planck Institute for Solid State Research, Stuttgart 70569, Germany; orcid.org/0000-0002-9923-5963

Alexander Hinderhofer – Institut für Angewandte Physik, Universität Tübingen, Tübingen 72076, Germany; orcid.org/0000-0001-8152-6386

Loïc C. Carbone – Laboratory of Photonics and Interfaces, École Polytechnique Fédérale de Lausanne, Lausanne 1015, Switzerland

Jacques-Edouard Moser – Photochemical Dynamics Group, École Polytechnique Fédérale de Lausanne, Lausanne 1015, Switzerland; orcid.org/0000-0003-0747-4666

Frank Schreiber – Institut für Angewandte Physik, Universität Tübingen, Tübingen 72076, Germany; orcid.org/0000-0003-3659-6718

Complete contact information is available at: <https://pubs.acs.org/doi/10.1021/acs.jpcllett.1c02937>

Author Contributions

The manuscript was written by A.D. with the support of J.V.M., M.A.H., D.M., L.M., and other coauthors. A.D.

conceptualized and led the study, prepared the samples, and conducted the analysis of the corresponding thin-films with the support of J.V.M. G.C.F. and J.-E.M. performed the transient absorption spectroscopy and the analysis; M.A.H. performed solid-state NMR spectroscopy and the analysis; whereas L.M., A.H., and F.S. performed GIWAXS measurements and the corresponding analysis. L.C.C. synthesized and characterized the organic spacers under the supervision of J.V.M., who together with D.M. contributed to the supervision of A.D., whereas J.M. and M.G. directed the project. All authors have approved the final manuscript.

Notes

The authors declare no competing financial interest.

Data presented here can be accessed at DOI: 10.5281/zenodo.5564724 under the license CC-BY-4.0 (Creative Commons Attribution-ShareAlike 4.0 International).

■ ACKNOWLEDGMENTS

A.D., D.M., J.M., and M.G. acknowledge the support from the Max Planck Society and the Max-Planck/EPFL Center. G.C.F. and J.-E.M. thank the SNSF (Grant No. 200021_175729) and NCCR-MUST for financial support. L.M., A.H., and F.S. acknowledge the European Synchrotron Radiation Facility (ESRF) for provision of synchrotron radiation facilities, and we would like to thank Oleg Kononov and Maciej Jankowski for assistance in using beamline ID10. We also thank Florian Bertram for assistance in using beamline P08 at PETRA III (DESY). Further, we acknowledge funding by the DFG within the framework of the SPP2196. J.V.M. is grateful for the Swiss National Science Foundation Grant No. 193174. M.A.H. is grateful for financial support from SNSF Grant No. 200020_178860. The authors thank Dr. Lukas Pfeifer (EPFL) for helpful discussions in the course of this study, as well as Aditya Mishra and Prof. Lyndon Emsley (EPFL) for supporting the solid-state NMR experiments.

■ REFERENCES

- (1) Jena, A. K.; Kulkarni, A.; Miyasaka, T. Halide Perovskite Photovoltaics: Background, Status, and Future Prospects. *Chem. Rev.* **2019**, *119*, 3036–3103.
- (2) Kim, J. Y.; Lee, J. W.; Jung, H. S.; Shin, H.; Park, N. G. High-Efficiency Perovskite Solar Cells. *Chem. Rev.* **2020**, *120*, 7867–7918.
- (3) Green, M. A.; Ho-Baillie, A.; Snaith, H. J. The Emergence of Perovskite Solar Cells. *Nat. Photonics* **2014**, *8*, 506–514.
- (4) Noh, J. H.; Im, S. H.; Heo, J. H.; Mandal, T. N.; Seok, S. I. Chemical Management for Colorful, Efficient, and Stable Inorganic-Organic Hybrid Nanostructured Solar Cells. *Nano Lett.* **2013**, *13*, 1764–1769.
- (5) Pellet, N.; Gao, P.; Gregori, G.; Yang, T.; Nazeeruddin, M. K.; Maier, J.; Grätzel, M. Mixed-Organic-Cation Perovskite Photovoltaics for Enhanced Solar-Light Harvesting. *Angew. Chem., Int. Ed.* **2014**, *53*, 3151–3157.
- (6) Hao, F.; Stoumpos, C. C.; Chang, R. P. H.; Kanatzidis, M. G. Anomalous Band Gap Behavior in Mixed Sn and Pb Perovskites Enables Broadening of Absorption Spectrum in Solar Cells. *J. Am. Chem. Soc.* **2014**, *136*, 8094–8099.
- (7) Saporov, B.; Mitzi, D. B. Organic-Inorganic Perovskites: Structural Versatility for Functional Materials Design. *Chem. Rev.* **2016**, *116*, 4558–4596.
- (8) Grancini, G.; Nazeeruddin, M. K. Dimensional Tailoring of Hybrid Perovskites for Photovoltaics. *Nat. Rev. Mater.* **2019**, *4*, 4–22.
- (9) Li, X.; Hoffman, J. M.; Kanatzidis, M. G. The 2D Halide Perovskite Rulebook: How the Spacer Influences Everything from the Structure to Optoelectronic Device Efficiency. *Chem. Rev.* **2021**, *121*, 2230–2291.

- (10) Gao, X.; Zhang, X.; Yin, W.; Wang, H.; Hu, Y.; Zhang, Q.; Shi, Z.; Colvin, V. L.; Yu, W. W.; Zhang, Y. Ruddlesden–Popper Perovskites: Synthesis and Optical Properties for Optoelectronic Applications. *Adv. Sci.* **2019**, *6*, 1900941.
- (11) Huang, P.; Kazim, S.; Wang, M.; Ahmad, S. Toward Phase Stability: Dion–Jacobson Layered Perovskite for Solar Cells. *ACS Energy Lett.* **2019**, *4*, 2960–2974.
- (12) Lin, Y.; Fang, Y.; Zhao, J.; Shao, Y.; Stuard, S. J.; Nahid, M. M.; Ade, H.; Wang, Q.; Shield, J. E.; Zhou, N.; Moran, A. M.; et al. Unveiling the Operation Mechanism of Layered Perovskite Solar Cells. *Nat. Commun.* **2019**, *10*, 1008.
- (13) Hu, Y.; Spies, L. M.; Alonso-Alvarez, D.; Mocherla, P.; Jones, H.; Hanisch, J.; Bein, T.; Barnes, P. R. F.; Docampo, P. Identifying and Controlling Phase Purity in 2D Hybrid Perovskite Thin Films. *J. Mater. Chem. A* **2018**, *6*, 22215–22225.
- (14) Liang, C.; Gu, H.; Xia, Y.; Wang, Z.; Liu, X.; Xia, J.; Zuo, S.; Hu, Y.; Gao, X.; Hui, W.; et al. Two-Dimensional Ruddlesden–Popper Layered Perovskite Solar Cells Based on Phase-Pure Thin Films. *Nat. Energy* **2021**, *6*, 38–45.
- (15) Dučinskas, A.; Kim, G. Y.; Moia, D.; Senocrate, A.; Wang, Y. R.; Hope, M. A.; Mishra, A.; Kubicki, D. J.; Siczek, M.; Bury, W.; et al. Unravelling the Behavior of Dion–Jacobson Layered Hybrid Perovskites in Humid Environments. *ACS Energy Lett.* **2021**, *6*, 337–344.
- (16) Milić, J. V. Multifunctional Layered Hybrid Perovskites. *J. Mater. Chem. C* **2021**, *9*, 11428.
- (17) Blancon, J. C.; Even, J.; Stoumpos, C. C.; Kanatzidis, M. G.; Mohite, A. D. Semiconductor Physics of Organic–Inorganic 2D Halide Perovskites. *Nat. Nanotechnol.* **2020**, *15*, 969–985.
- (18) Wang, Y.; Senocrate, A.; Mladenović, M.; Dučinskas, A.; Kim, G. Y.; Röthlisberger, U.; Milić, J. V.; Moia, D.; Grätzel, M.; Maier, J. Photo De-Mixing in Dion–Jacobson Two-Dimensional Mixed Halide Perovskites. *arXiv*; <http://arxiv.org/abs/2107.01260>, 2021.
- (19) Mathew, P. S.; Dubose, J. T.; Cho, J.; Kamat, P. V. Spacer Cations Dictate Photoinduced Phase Segregation in 2D Mixed Halide Perovskites. *ACS Energy Lett.* **2021**, *6*, 2499–2501.
- (20) Ahmad, S.; Fu, P.; Yu, S.; Yang, Q.; Liu, X.; Wang, X.; Wang, X.; Guo, X.; Li, C. Dion–Jacobson Phase 2D Layered Perovskites for Solar Cells with Ultrahigh Stability. *Joule* **2019**, *3*, 1–13.
- (21) Yao, Z.; Zhou, Y.; Yin, X.; Li, X.; Han, J.; Tai, M.; Zhou, Y.; Li, J.; Hao, F.; Lin, H. Role of Alkyl Chain Length in Diaminoalkane Linked 2D Ruddlesden–Popper Halide Perovskites. *CrystEngComm* **2018**, *20*, 6704–6712.
- (22) Safdari, M.; Svensson, P. H.; Hoang, M. T.; Oh, I.; Kloo, L.; Gardner, J. M. Layered 2D Alkyldiammonium Lead Iodide Perovskites: Synthesis, Characterization, and Use in Solar Cells. *J. Mater. Chem. A* **2016**, *4*, 15638–15646.
- (23) Hu, J.; Oswald, I. W. H.; Stuard, S. J.; Nahid, M. M.; Zhou, N.; Williams, O. F.; Guo, Z.; Yan, L.; Hu, H.; Chen, Z.; et al. Synthetic Control over Orientational Degeneracy of Spacer Cations Enhances Solar Cell Efficiency in Two-Dimensional Perovskites. *Nat. Commun.* **2019**, *10*, 1276.
- (24) Du, K. Z.; Tu, Q.; Zhang, X.; Han, Q.; Liu, J.; Zauscher, S.; Mitzi, D. B. Two-Dimensional Lead(II) Halide-Based Hybrid Perovskites Templated by Acene Alkylamines: Crystal Structures, Optical Properties, and Piezoelectricity. *Inorg. Chem.* **2017**, *56*, 9291–9302.
- (25) Mao, L.; Tsai, H.; Nie, W.; Ma, L.; Im, J.; Stoumpos, C. C.; Malliakas, C. D.; Hao, F.; Wasielewski, M. R.; Mohite, A. D.; et al. Role of Organic Counterion in Lead- and Tin-Based Two-Dimensional Semiconducting Iodide Perovskites and Application in Planar Solar Cells. *Chem. Mater.* **2016**, *28*, 7781–7792.
- (26) Li, X.; Ke, W.; Traoré, B.; Guo, P.; Hadar, I.; Kepenekian, M.; Even, J.; Katan, C.; Stoumpos, C. C.; Schaller, R. D.; et al. Two-Dimensional Dion–Jacobson Hybrid Lead Iodide Perovskites with Aromatic Diammonium Cations. *J. Am. Chem. Soc.* **2019**, *141*, 12880–12890.
- (27) Gélvez-Rueda, M. C.; Van Gompel, W. T. M.; Herckens, R.; Lutsen, L.; Vanderzande, D.; Grozema, F. C. Inducing Charge Separation in Solid-State Two-Dimensional Hybrid Perovskites through the Incorporation of Organic Charge-Transfer Complexes. *J. Phys. Chem. Lett.* **2020**, *11*, 824–830.
- (28) Passarelli, J. V.; Fair, D. J.; Sather, N. A.; Hendricks, M. P.; Sai, H.; Stern, C. L.; Stupp, S. I. Enhanced Out-of-Plane Conductivity and Photovoltaic Performance in $n = 1$ Layered Perovskites through Organic Cation Design. *J. Am. Chem. Soc.* **2018**, *140*, 7313.
- (29) Quan, L. N.; Yuan, M.; Comin, R.; Voznyy, O.; Beauregard, E. M.; Hoogland, S.; Buin, A.; Kirmani, A. R.; Zhao, K.; Amassian, A.; et al. Ligand-Stabilized Reduced-Dimensionality Perovskites. *J. Am. Chem. Soc.* **2016**, *138*, 2649–2655.
- (30) Zhang, X.; Wu, G.; Fu, W.; Qin, M.; Yang, W.; Yan, J.; Zhang, Z.; Lu, X.; Chen, H. Orientation Regulation of Phenylethylammonium Cation Based 2D Perovskite Solar Cell with Efficiency Higher Than 11%. *Adv. Energy Mater.* **2018**, *8*, 1702498.
- (31) Lemmerer, A.; Billing, D. G. Two Packing Motifs Based upon Chains of Edge-Sharing PbI_6 Octahedra. *Acta Crystallogr., Sect. C: Cryst. Struct. Commun.* **2006**, *62*, 597–601.
- (32) Li, Y.; Milic, J. V.; Ummadisingu, A.; Seo, J.; Im, J.; Kim, H.; Liu, Y.; Dar, M. I.; Zakeeruddin, S. M.; Wang, P.; et al. Bifunctional Organic Spacers for Formamidinium-Based Hybrid Dion–Jacobson Two-Dimensional Perovskite Solar Cells. *Nano Lett.* **2019**, *19*, 150–157.
- (33) Gélvez-Rueda, M. C.; Ahlawat, P.; Merten, L.; Jahanbakhshi, F.; Mladenović, M.; Hinderhofer, A.; Dar, M. I.; Li, Y.; Dučinskas, A.; Carlsen, B.; et al. Formamidinium-Based Dion–Jacobson Layered Hybrid Perovskites: Structural Complexity and Optoelectronic Properties. *Adv. Funct. Mater.* **2020**, *30*, 2003428.
- (34) Hou, M.; Xu, Y.; Zhou, B.; Tian, Y.; Wu, Y.; Zhang, D.; Wang, G.; Li, B.; Ren, H.; Li, Y.; et al. Aryl Diammonium Iodide Passivation for Efficient and Stable Hybrid Organ–Inorganic Perovskite Solar Cells. *Adv. Funct. Mater.* **2020**, *30*, 2002366.
- (35) Jahanbakhshi, F.; Mladenović, M.; Dankl, M.; Boziki, A.; Ahlawat, P.; Röthlisberger, U. Organic Spacers in 2D Perovskites: General Trends and Structure–Property Relationships from Computational Studies. *Helv. Chim. Acta* **2021**, *104*, No. e2000232.
- (36) Sapurina, I.; Stejskal, J. The Mechanism of the Oxidative Polymerization of Aniline and the Formation of Supramolecular Polyaniline Structures. *Polym. Int.* **2008**, *57*, 1295–1325.
- (37) Zheng, Y.; Niu, T.; Qiu, J.; Chao, L.; Li, B.; Yang, Y.; Li, Q.; Lin, C.; Gao, X.; Zhang, C.; et al. Oriented and Uniform Distribution of Dion–Jacobson Phase Perovskites Controlled by Quantum Well Barrier Thickness. *Sol. RRL* **2019**, *3*, 1900090.
- (38) Gómez, V.; Klyatskaya, S.; Fuhr, O.; Kalytchuk, S.; Zbořil, R.; Kappes, M.; Lebedkin, S.; Ruben, M. Pressure-Modulated Broadband Emission in 2D Layered Hybrid Perovskite-Like Bromoplumbate. *Inorg. Chem.* **2020**, *59*, 12431–12436.
- (39) Kubicki, D. J.; Stranks, S. D.; Grey, C. P.; Emsley, L. NMR Spectroscopy Probes Microstructure, Dynamics and Doping of Metal Halide Perovskites. *Nat. Rev. Chem.* **2021**, *5*, 624.
- (40) Piveteau, L.; Morad, V.; Kovalenko, M. V. Solid-State NMR and NQR Spectroscopy of Lead-Halide Perovskite Materials. *J. Am. Chem. Soc.* **2020**, *142*, 19413–19437.
- (41) Lee, J.; Lee, W.; Kang, K.; Lee, T.; Lee, S. K. Layer-by-Layer Structural Identification of 2D Ruddlesden–Popper Hybrid Lead Iodide Perovskites by Solid-State NMR Spectroscopy. *Chem. Mater.* **2021**, *33*, 370–377.
- (42) Su, T. S.; Eickemeyer, F. T.; Hope, M. A.; Jahanbakhshi, F.; Mladenović, M.; Li, J.; Zhou, Z.; Mishra, A.; Yum, J. H.; Ren, D.; et al. Crown Ether Modulation Enables over 23% Efficient Formamidinium-Based Perovskite Solar Cells. *J. Am. Chem. Soc.* **2020**, *142*, 19980–19991.
- (43) Aebli, M.; Piveteau, L.; Nazarenko, O.; Benin, B. M.; Krieg, F.; Verel, R.; Kovalenko, M. V. Lead-Halide Scalar Couplings in ^{207}Pb NMR of APbX_3 Perovskites ($A = \text{Cs}$, Methylammonium, Formamidinium; $X = \text{Cl}$, Br , I). *Sci. Rep.* **2020**, *10*, 8229.
- (44) Merten, L.; Hinderhofer, A.; Baumeler, T.; Arora, N.; Hagenlocher, J.; Zakeeruddin, S. M.; Dar, M. I.; Grätzel, M.; Schreiber, F. Quantifying Stabilized Phase Purity in Formamidinium-

Based Multiple-Cation Hybrid Perovskites. *Chem. Mater.* **2021**, *33*, 2769–2776.

(45) Zhang, K.; Zhang, M.; Zhu, N.; Yin, H.; Xing, J.; Wang, L. Effects of Organic Ligands on Efficiency and Stability of Perovskite Light-Emitting Diodes. *J. Mater. Sci.* **2021**, *56*, 11436–11447.

(46) Sichert, J. A.; Hemmerling, A.; Cardenas-Daw, C.; Urban, A. S.; Feldmann, J. Tuning the Optical Bandgap in Layered Hybrid Perovskites through Variation of Alkyl Chain Length. *APL Mater.* **2019**, *7*, 041116.

(47) Ishihara, T.; Takahashi, J.; Goto, T. Optical Properties Due to Electronic Transitions in Two-Dimensional Semiconductors ($C_nH_{2n+1}NH_3$)₂PbI₄. *Phys. Rev. B: Condens. Matter Mater. Phys.* **1990**, *42*, 11099–11107.

(48) Liu, G.; Gong, J.; Kong, L.; Schaller, R. D.; Hu, Q.; Liu, Z.; Yan, S.; Yang, W.; Stoumpos, C. C.; Kanatzidis, M. G.; et al. Isothermal Pressure-Derived Metastable States in 2D Hybrid Perovskites Showing Enduring Bandgap Narrowing. *Proc. Natl. Acad. Sci. U. S. A.* **2018**, *115*, 8076–8081.

(49) Liu, S.; Sun, S.; Gan, C. K.; Del Águila, A. G.; Fang, Y.; Xing, J.; Thu Ha Do, T.; White, T. J.; Li, H.; Huang, W.; et al. Manipulating Efficient Light Emission in Two-Dimensional Perovskite Crystals by Pressure-Induced Anisotropic Deformation. *Sci. Adv.* **2019**, *5*, No. eaav9445.

(50) Blancon, J.; Stier, A. V.; Tsai, H.; Nie, W.; Stoumpos, C. C.; Traoré, B.; Pedesseau, L.; Kepenekian, M.; Katsutani, F.; Noe, G. T.; et al. Scaling Law for Excitons in 2D Perovskite Quantum Wells. *Nat. Commun.* **2018**, *9*, 2254.

(51) Wang, G. E.; Wang, M. S.; Jiang, X. M.; Liu, Z. F.; Lin, R. G.; Cai, L. Z.; Guo, G. C.; Huang, J. S. Crystal Structures and Optical Properties of 1-D Iodoplumbates Templated by in Situ Synthesized p-Phenylenediamine Derivatives. *Inorg. Chem. Commun.* **2011**, *14*, 1957–1961.

(52) Kamminga, M. E.; Fang, H.-H.; Filip, M. R.; Giustino, F.; Baas, J.; Blake, G. R.; Loi, M. A.; Palstra, T. T. M. Confinement Effects in Low-Dimensional Lead Iodide Perovskite Hybrids. *Chem. Mater.* **2016**, *28*, 2.

(53) Roiati, V.; Mosconi, E.; Listorti, A.; Colella, S.; Gigli, G.; De Angelis, F. Stark Effect in Perovskite/TiO₂ Solar Cells: Evidence of Local Interfacial Order. *Nano Lett.* **2014**, *14*, 2168–2174.

(54) Queloz, V. I. E.; Bouduban, M. E. F.; García-Benito, I.; Fedorovskiy, A.; Orlandi, S.; Cavazzini, M.; Pozzi, G.; Trivedi, H.; Lupascu, D. C.; Beljonne, D.; et al. Spatial Charge Separation as the Origin of Anomalous Stark Effect in Fluorous 2D Hybrid Perovskites. *Adv. Funct. Mater.* **2020**, *30*, 2000228.

(55) Walters, G.; Wei, M.; Voznyy, O.; Quintero-Bermudez, R.; Kiani, A.; Smilgies, D. M.; Munir, R.; Amassian, A.; Hoogland, S.; Sargent, E. The Quantum-Confined Stark Effect in Layered Hybrid Perovskites Mediated by Orientational Polarizability of Confined Dipoles. *Nat. Commun.* **2018**, *9*, 4214.

(56) Sharma, D. K.; Hirata, S.; Biju, V.; Vacha, M. Stark Effect and Environment-Induced Modulation of Emission in Single Halide Perovskite Nanocrystals. *ACS Nano* **2019**, *13*, 624–632.

(57) Cappel, U. B.; Feldt, S. M.; Schöneboom, J.; Hagfeldt, A.; Boschloo, G. The Influence of Local Electric Fields on Photoinduced Absorption in Dye-Sensitized Solar Cells. *J. Am. Chem. Soc.* **2010**, *132*, 9096–9101.

(58) Giovanni, D.; Chong, W. K.; Dewi, H. A.; Thirumal, K.; Neogi, I.; Ramesh, R.; Mhaisalkar, S.; Mathews, N.; Sum, T. C. Tunable Room-Temperature Spin-Selective Optical Stark Effect in Solution-Processed Layered Halide Perovskites. *Sci. Adv.* **2016**, *2*, No. e1600477.

(59) Jong, U. G.; Yu, C. J.; Ri, G. C.; McMahon, A. P.; Harrison, N. M.; Barnes, P. R. F.; Walsh, A. Influence of Water Intercalation and Hydration on Chemical Decomposition and Ion Transport in Methylammonium Lead Halide Perovskites. *J. Mater. Chem. A* **2018**, *6*, 1067–1074.

(60) Svane, K. L.; Forse, A. C.; Grey, C. P.; Kieslich, G.; Cheetham, A. K.; Walsh, A.; Butler, K. T. How Strong Is the Hydrogen Bond in Hybrid Perovskites? *J. Phys. Chem. Lett.* **2017**, *8*, 6154–6159.

(61) Spanopoulos, I.; Hadar, I.; Ke, W.; Tu, Q.; Chen, M.; Tsai, H.; He, Y.; Shekhawat, G.; Dravid, V. P.; Wasielewski, M. R.; et al. Uniaxial Expansion of the 2D Ruddlesden-Popper Perovskite Family for Improved Environmental Stability. *J. Am. Chem. Soc.* **2019**, *141*, 5518–5534.

(62) Cohen, B. El; Wierzbowska, M.; Etgar, L. High Efficiency Quasi 2D Lead Bromide Perovskite Solar Cells Using Various Barrier Molecules. *Sustain. Energy Fuels* **2017**, *1*, 1935–1943.